THE RELATIONSHIP BETWEEN DETECTION ALGORITHMS FOR HYPERSPECTRAL AND RADAR APPLICATIONS

Nirmal Keshava, Stephen M. Kogon, Dimitris Manolakis

MIT Lincoln Laboratory
244 Wood Street Lexington, MA 02420-9185
keshava@ll.mit.edu, (o) (781) 981-3344

ABSTRACT

Hyperspectral data consists of hundreds of contiguous radiometric measurements collected passively from each pixel in a scene. Detection capitalizes on exploiting the difference between target and background spectral signatures. Many detection methods in hyperspectral processing employ signal models commonly used in radar even though it is an active sensor. Starting from a common signal model, we discuss adaptive detection algorithms for hyperspectral data by outlining fundamental similarities and differences with radar. We demonstrate detection using hyperspectral data through experiments with real data and discuss the fundamental applicability of adaptive radar signal models to detection in hyperspectral processing.

1. INTRODUCTION

The potential of hyperspectral sensors to perform target detection has begun to emerge as data from current and projected sensors has shown that passive, spectral measurements can distinguish targets from background. The basis for detection resides in exploiting the differences in reflective properties that occur in the hundreds of contiguous spectral bands that comprise hyperspectral signals. Collectively, these measurements constitute a vector signal that may be used in detection algorithms designed to maximize the separation between target and background signals.

For detection algorithms to be successful in operational scenarios, they must employ accurate statistical descriptions of both the target and background. Many of the algorithms currently in use have been adapted from signal models used for detection in radar systems. Consequently, despite the significant differences in the physical mechanisms, a strong parallelism can be drawn that maps the measured signals from each sensor to a common signal model.

This work was sponsored by the Department of the Defense under Contract F19628-00-C-0002. Opinions, interpretations, conclusions, and recommendations are those of the author and are not necessarily endorsed by the United States Air Force.

2. MODELS FOR HYPERSPECTRAL SENSING AND MTI RADAR

In order to understand the relationship between the signal models for hyperspectral sensing and MTI radar, we first explain the basic concepts behind both sensor models.

2.1. Hyperspectral Imaging

Hyperspectral sensors passively collect measurements of radiation in hundreds of contiguous spectral bands. Collectively, hyperspectral imaging (HSI) provides continuous coverage of the electromagnetic spectrum over a wide range of wavelengths. Incident radiation from the sun follows several pathways as it reaches the sensor where it is measured in terms of *radiance* (Watts/steradian/cm^2/μm). Mathematically, the radiance arriving at the sensor, $L_{sensor}(\lambda)$, can be described as

$$L_{sensor}(\lambda) = L_{solar}(\lambda)\rho(\lambda)\tau(\lambda) + L_{path}(\lambda) \quad (1)$$

where $L_{solar}(\lambda)$ is the radiance spectrum entering the atmosphere at a designated time and location as a function of wavelength. $\tau(\lambda)$ is the atmospheric transmittance, and $\rho\lambda$ is the surface reflectance, and $L_{path}(\lambda)$ is the additive path radiance arising from interactions with the atmosphere.

In some cases, processing of the radiance arriving at the sensor can yield useful results. However, in most cases, the surface reflectance, $\rho(\lambda)$, is the quantity that is desired because it is an intrinsic property of the area being imaged and is invariant to differences in atmospheric conditions during observation. Reflectance is defined as the ratio of the intensity arriving at the surface of an object to the intensity reflected ($0 \leq \rho(\lambda) \leq 1$), and the recovery of $\rho(\lambda)$ from $L(\lambda)$ is accomplished through *atmospheric compensation.* In this procedure, the surface reflectance for each pixel is recovered by removing the effects of gaseous and water vapor absorption in the atmosphere. Atmospheric compensation is derived from radiative transfer models and is by no means an exact science. In addition to being computationally demanding, the amount of error in the compensation is

Fig. 1. 3-D datacubes for HSI.

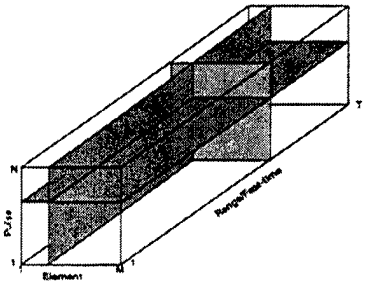

Fig. 2. 3-D CPI datacube for MTI radar.

difficult to quantify. Nevertheless, most hyperspectral processing is performed "in reflectance."

Hyperspectral sensors collect data along two spatial axes derived from the motion of the sensor (along-track and across-track) and another spectral axis. The resulting three-dimension cube is depicted in Figure 1. The spatial resolution in HSI is a consequence of several factors, but generally can be determined from only two: instantaneous field of view (IFOV) and altitude. IFOV is a parameter describing the optics that conveys the angular expanse of one element on the focal plane array that measures radiance. Multiplying the IFOV by the altitude of the sensor gives the pixel size of the scene.

2.1.1. Linear Mixing Model

Hyperspectral processing attempts to exploit the wavelength-dependent features of the reflectance spectrum measured from a pixel. However, it is quite common for the surface area occupying a pixel to be a combination of distinct materials, or endmembers (e.g., water, trees, vehicle), each possessing their own reflectance functions. The reflectance function of a mixed pixel is some combination of the distinct reflectance functions of each endmember. In general, accurate physical modelling of the reflective properties of mixtures is not trivial, and is a function of numerous molecular parameters, as well, as the proportions in which the endmembers appear. Several physically-derived models have been proposed to model mixing under different conditions.

A common assumption for describing the mixing process throughout hyperspectral processing that is analytically tractable is that the reflectance spectrum of a mixed pixel is a weighted linear combination of the individual endmember reflectance functions, where the weights are the proportions in which each endmember appears. Thus, the mathematical model describing this recipe for a mixed pixel is

$$\mathbf{x} = \mathbf{S}\mathbf{a} + \mathbf{n} = \sum_{i=1}^{P} a_i \mathbf{s}_i + \mathbf{n} \qquad (2)$$

Here, $\mathbf{x}$ is the reflectance spectrum of a mixed pixel, and $\mathbf{S}$ is a matrix whose P columns are the reflectance spectra of the endmembers, and $\mathbf{a}$ is a $P \times 1$ vector of non-negative fractional abundances. The additive noise vector, $\mathbf{n}$, represents the inaccuracies in the model. Two important constraints on $\mathbf{a}$ must be imposed. The *non-negativity* constraint demands that $a_i \geq 0, i = 1, ..., P$, and to ensure the composition of a mixed pixel is completely accounted for, the *additivity* constraint requires $\sum_{i=1}^{P} a_i = 1$. Collectively, these constraints and the synthesis equation for mixed pixels in (2) are referred to as the Linear Mixing Model (LMM).

2.2. MTI Radar

The objective of MTI radar systems is to detect the presence of moving objects. MTI radars on airborne platforms illuminate a scene with a waveform and sample the return at each element of a multi-element array (We restrict our attention to uniform linear arrays (ULA).). The process is repeated during a coherent processing interval (CPI). After pulse compression, the data is organized into a three-dimensional CPI datacube, as depicted in Figure 2, that is indexed by 1) pulse number, 2) element number, and 3) sample number (range).

At each range value, a two-dimensional function locates the presence of reflecting objects by their cone angle and their corresponding Doppler frequency. For a fixed system, the signal strength returned by a target depends upon its range cross-section (RCS) value and its range. Stationary objects will yield values along a "clutter ridge", whereas moving objects will lie off the ridge by an amount proportional to its velocity relative to the platform. A moving target is most visible when its velocity is high (so as to move it as far away as possible from the clutter ridge), and when it returns a strong signal.

By virtue of linearity, MTI radar observes a signal model similar to the LMM in (2). The vector signal measured by an antenna array is the linear superposition of reflections received from all directions, and when a target is present, the corresponding signal is given by

$$\mathbf{x} = \mathbf{t} + \mathbf{c} + \mathbf{n}. \tag{3}$$

Here, $\mathbf{x}$ is an $M \times 1$ observation vector, where M is the number of elements on the ULA, $\mathbf{c}$ and $\mathbf{n}$ are clutter and noise, respectively, and $\mathbf{t}$ is the target and is expressed as $\mathbf{t} = \alpha\mathbf{v}(\phi, f)$. α is the relative amplitude of the return signal, and $\mathbf{v}$ is the steering vector which is related to the geometry of the ULA as well as signal parameters. The entries of $\mathbf{v}$ are given by:

$$v_{mn} = e^{j2\pi[(m-1)\frac{f}{\mathrm{PRF}} + (n-1)\frac{d}{\lambda}\cos\phi]} \tag{4}$$

where $m = 1, ..., M$, is the element number, $n = 1, ..., N$, is the pulse number, ϕ is the azimuth angle, f is the Doppler frequency, λ is the wavelength, d is the array element spacing, and PRF is the pulse repetition frequency. Resolution in MTI radar systems is driven in the range direction by the signal bandwidth of the interrogating signal and by the aperture length in azimuth.

2.3. Relationships Between HSI and MTI Radar

We can see from (2) and (3) that signal models for HSI and MTI radar are quite similar. Both sensors organize measurements that occupy three axes (See Figures 1 and 2). Despite the fact that HSI is passive and yields non-negative vector measurements, and MTI radar is a form of active sensing producing complex-values, the key to this equivalence is the parallelism between endmembers and steering vectors as well as RCS and fractional abundances.

In (4), $\mathbf{v}$ is a vector whose structure gives rise to the complex-valued signal in $\mathbf{x}$. When a target is in motion at a specific range, its location in azimuth and Doppler frequency decide the exact value of the steering vector. The one-dimensional subspace defined by the target vector, $\mathbf{t}$, varies depending on the location and speed of the target. In most instances, the resolution cell size is sufficiently small that only one moving target resides in it. In the case, however, where multiple moving targets reside in a single cell, the response from the cell will be the sum of weighted steering vectors, each having their own Doppler frequency. The target response, $\mathbf{t}$, can be extended to include P targets, so that $\mathbf{t} = \sum_{i=1}^{P} \alpha_i \mathbf{v}_i = \mathbf{V}\mathbf{a}$. Compared to (2), the steering vectors that are columns of $\mathbf{V}$ are analogous to the endmembers in $\mathbf{S}$. Further, in (4), $\mathbf{c}$ and $\mathbf{n}$ are comparable to the background and additive noise in (2), and their statistics are key factors in the detectors for each sensor type.

3. TARGET DETECTION

Based on the comparable signal models for HSI and MTI radar discussed in Section 2, we can consider strategies for detection in each. The LMM has been employed in numerous circumstances to describe the mixing process. For the purpose of target detection, it is capable of conveying the mathematical relationship between the spectra of targets and background. By virtue of the LMM, we assume that all pixels in a scene imaged by a hyperspectral sensor consist of at least one endmember from the columns of $\mathbf{S}$.

A specific type of target possesses a spectrum, but variability can arise due to many factors, including changes in observation conditions. Depending on its source, variability can be accounted for by adding endmembers (and corresponding abundances) to describe the same target under different conditions, or by shaping the additive noise, $\mathbf{n}$, in the LMM to reflect statistical variability. $\mathbf{S}_t$ denotes the subset of columns in $\mathbf{S}$ describing targets, and $\mathbf{S}_b$ denotes background endmembers. Because the entries of $\mathbf{S}$ are non-negative, $\mathbf{S}_t$ and $\mathbf{S}_b$ cannot be mutually orthogonal spaces, and the subspaces they span necessarily overlap.

3.1. Types of Hyperspectral Detection

The task of detection can be posed for two separate circumstances that are of interest in hyperspectral processing [1]. The **Known Target** detection problem occurs when the presence of a specific target is to be detected amid background and noise, and $\mathbf{S}_t$ is known. In contrast the **Unknown Target** detection problem has no knowledge of a target subspace, but attempts to detect any pixel that is different from the background. For this reason, detectors designed for this goal are often called *anomaly* detectors.

The class of **Known Target** detection algorithms can be further divided into two categories. The set of **structured background** algorithms assumes that the subspace where the background resides, $\mathbf{S}_b$, is known so that the LMM in (2) can be re-written as

$$\mathbf{x} = \mathbf{S}_t\mathbf{a}_t + \mathbf{S}_b\mathbf{a}_b + \mathbf{n} \tag{5}$$

$$= \sum_{i=1}^{P_T} a_i\mathbf{s}_i + \sum_{i=P_T+1}^{P_B+P_T} a_i\mathbf{s}_i + \mathbf{n} \tag{6}$$

where $P = P_T + P_B$. Note that the obstacles to perfect detection, background and additive noise, have been modelled as two distinct entities, $\mathbf{S}_b\mathbf{a}_b$ and $\mathbf{n}$. The resulting binary detection test for structured background is

$$\mathbf{H}_0 : \quad \mathbf{x} = \mathbf{S}_b\mathbf{a}_b + \mathbf{n} \tag{7}$$

$$\mathbf{H}_1 : \quad \mathbf{x} = \mathbf{S}_t\mathbf{a}_t + \mathbf{S}_b\mathbf{a}_b + \mathbf{n} \tag{8}$$

Alternatively, if the background endmembers are unknown, the sources of interference cannot be separated into

separate background and noise terms. The **unstructured background** problem lumps all non-target pixel contributions into a single vector, $\mathbf{w}$, and the resulting binary detection test is written as:

$$\mathbf{H}_0: \quad \mathbf{x} = \mathbf{w} \tag{9}$$

$$\mathbf{H}_1: \quad \mathbf{x} = \mathbf{S}_t\mathbf{a}_t + \mathbf{w} \tag{10}$$

The different pairs of hypotheses in (7-8) and (9-10) convey varying levels of knowledge about the detection problem and are critical to the formulation of optimal detectors.

When the size of a target is expected to be equal to or greater in size than that of a pixel, i.e., the target is resolved, the background is no longer present in either hypothesis. This is a significant departure from radar detection models which assume an *additive* target appears in addition to clutter. A *replacement* target displaces some amount, or all, of the environmental interference, or background. The fact that the amount of background displaced by a target in a mixed pixel can vary means that the statistics of the interference will also vary. As a consequence, the foremost challenge in the design of optimal, statistical detectors for subpixel targets stems from the uncertainty of what fraction of the pixel the target occupies.

3.2. MTI Detection

Like the techniques for hyperspectral detection, algorithms in MTI radar find moving targets by exposing the Doppler effect in signals measured by a ULA. Just as the subspaces defined by target and background endmembers in HSI detection provide the basis for separating target and background pixels, the geometry of the array, along with the signal parameters, are combined by algorithms to maximize the visibility of moving targets.

Algorithms for detecting $\mathbf{t}$ in (3) optimally suppress the presence of $\mathbf{c}$ and $\mathbf{n}$ by means of Space-Time Adaptive Processing (STAP) [2]. Resembling the detection model for a known target in an unstructured background, the binary detection model for a moving target, $\mathbf{t}$, is given by

$$\mathbf{H}_0: \quad \mathbf{x} = \mathbf{w} \tag{11}$$

$$\mathbf{H}_1: \quad \mathbf{x} = \mathbf{t} + \mathbf{w}, \tag{12}$$

where $\mathbf{w} = \mathbf{c} + \mathbf{n}$ in (3).

Moving targets may be present at any range and azimuth position, and each pixel in the MTI radar datacube is a candidate for a detection test. For a specific range value, the cube of MTI data reduces to a single plane having MN resolution cells. It is well known that the detector which maximizes the SNR whitens the received signal based on a filter derived from the covariance of the interference. A covariance, $\mathbf{R}_w$, having size $MN \times MN$ introduces significant complications, and, most often, a local covariance of a smaller size is generated from a local neighborhood around the cell being processed. Confining the covariance to a neighborhood reduces the possibility of introducing nonstationary behavior and results in a more precise estimate.

3.3. Relationship Between HSI and MTI Detection

As noted earlier, reflectance values in hyperspectral processing are non-negative and no greater than one, and unlike the intuition from radar, targets do not necessarily induce signals of greater magnitude than background. Rather, targets are discerned from background reflectance spectra primarily by their shape, and detectors exploit the differences in spectral shapes represented by the endmembers to separate targets from background.

3.4. Detectors

We have shown that the signal models for hyperspectral target detection in (7-8) and (9-10) and the signal model for the detection of moving targets in (1112) are simialr. The key to the parallelism lies in the similar roles played by endmembers and steering vectors and the equivalence of abundances and RCS values and is further driven by the assumption of linearity when combining multiple signals.

By (11-11), detection in MTI radar compares range-angle cells to a threshold to determine whether or not a target is moving. Numerous detectors have been proposed to perform this comparison, each equipped to adaptively optimize some aspect of the decision. Notably, the most desirable features of detectors are: 1) CFAR (Constant False Alarm Rate), 2) maximum SNR, and 3) speed of computation. A detector might be able to assure one of these features, at the expense of maintaining the others, and the trade-off of these qualities is instrumental to an appropriate implementation.

The same set of circumstances also surrounds hyperspectral detection. A taxonomy of hyperspectral detectors for both the known and unknown target case hyperspectral data appears in [1], indicating the hierarchy of common detectors. The Generalized Likelihood Ratio Test (GLRT) [3] is a CFAR detector that utilizes the unstructured background signal model, and for a single known target spectrum, $\mathbf{s}$, the GLRT for a test pixel spectrum, $\mathbf{x}$, is given by:

$$\mathcal{T}_{GLRT}(\mathbf{x}) = \frac{(\mathbf{s}^T\overline{\mathbf{R}_w}^{-1}\mathbf{x})^2}{(\mathbf{s}^T\overline{\mathbf{R}_w}^{-1}\mathbf{s})(1+\mathbf{x}^T\overline{\mathbf{R}_w}^{-1}\mathbf{x})} \underset{H_0}{\overset{H_1}{\gtrless}} \eta_0. \tag{13}$$

Other familiar detectors may be derived directly from the GLRT under specific circumstances, such as the Adaptive Matched Filter (AMF) [3] and the Adaptive Coherence Estimator (ACE) [4, 5]. In the improbable case where the interference covariance is the identity matrix, the ACE simplifies to a simple cosine measure between $\mathbf{s}$ and $\mathbf{x}$, often

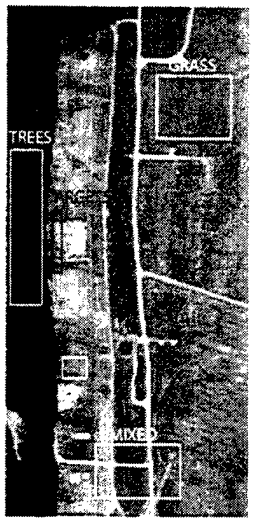

Fig. 3. Forest Radiance I scene.

referred to in the hyperspectral processing literature as the Spectral Angle Mapper (SAM). It is defined as:

$$\mathcal{T}_{SAM}(\mathbf{x}) = \frac{\mathbf{s}^t\mathbf{x}}{\sqrt{\mathbf{s}^T\mathbf{s}}\sqrt{\mathbf{x}^T\mathbf{x}}} \qquad (14)$$

With no incorporation of background statistics, clearly, SAM cannot be CFAR or optimum in any sense.

4. HYPERSPECTRAL DETECTION RESULTS

Figure 3 displays the RGB image of the Forest Radiance I scene imaged by the (Hyperspectral Digital Imagery Collection Experiment) HYDICE sensor. The data collection acquired 210 bands of spectral data in spectral bins $3-11$ nm wide ranging from $399-2501$ nm (Visible to Shortwave Infrared). The scene consists of 1280 lines of data, each having 320 samples with approximately 1 m $\times$ 1 m spatial resolution. Three regions of distinct background type have been demarcated: trees, grass, and mixed. In addition, a separate region is outlined encompassing several vehicles of the same type, from which pure target pixels are derived. Figure 4(a) illustrates the mean target spectrum obtained from 37 pure target pixels.

We demonstrate detection with hyperspectral data in two different experiments. The goal of the first experiment is to demonstrate how sub-pixel targets are detected when they appear mixed with background. The second experiment considers the extreme case of the sub-pixel target problem when the target is resolved and obscures all background when it is present. For both experiments, the performance of the SAM and GLRT detectors is compared side-by-side.

4.1. Sub-pixel Targets

Sub-pixel target spectra have been created synthetically by adding the pure mean target spectrum from Figure 4(a) in varying proportions to the 8232 pure tree spectra (background) in Figure 3. Although, there is no assurance that spectra mix linearly in real mixed pixels, we have employed this assumption for our investigation until accurate sub-pixel target data and ground truth become available.

We have estimated the background covariance from the homogeneous tree spectra. Both detectors yield values between 0 (background) and 1 (target), and pure background detection statistic values have been generated from the 8232 tree pixels. An equal number of target mixtures resulted by combining the same background pixels with the mean target vehicle spectrum in 25%/75%, 50%/50%, and 75%/25% target/background proportions. The range of detection statistic values for the SAM detector appears in Figure 4(b) and for the GLRT in Figure 4(c).

In Figures 4(b) and 4(c), the regions of dark blue correspond to the range of statistic values induced by the tree pixels. The regions of red correspond to the range of target mixture statistic values. Intervals of light blue, if any, correspond to regions where test statistics from pure background pixels and sub-pixel targets overlap and indicate pixels where false alarms and missed detections could occur. A white strip appears at the value of the mean target/background statistic. Regions of yellow indicate the amount of separation, if any, between target and background. The greater the width of the yellow region, the better the detector is capable of separating sub-pixel targets from pure background.

4.2. Resolved Targets

The 37 target pixels in Figure 3 are fully resolved, and they completely obscure any background. In spite of the fact that there is no background to whiten when the target is present, and using the 37 target pixels and the 8232 background pixels, we assessed the performance of the SAM and GLRT detectors in separating pure target and pure background spectra. In Figure 4(d), both the SAM and GLRT detection results for resolved targets are depicted side-by-side.

4.3. Discussion

In Figure 4(b) the SAM detector is unable to successfully separate every sub-pixel target until 75% of the pixel is occupied by the target. This is not surprising since SAM does nothing to suppress the background. On the other hand, in Figure 4(c), the GLRT has a relatively large pure background and target/background separation even when the target occupies only 25% of the pixel. This is due to the suppression of the background through whitening by the in-

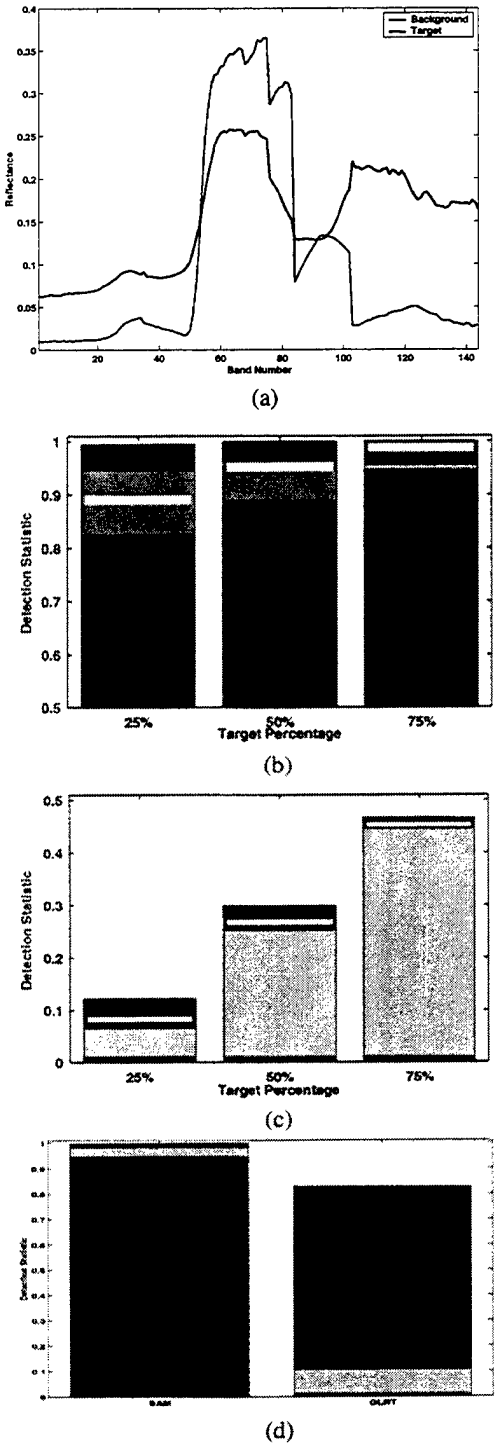

Fig. 4. (a) Mean target spectrum; (b) Sub-pixel detection statistics for SAM; (c) Sub-pixel detection statistics for GLRT; (d) Resolved target detection results for SAM and GLRT.

verse covariance, $\mathbf{R}_w^{-1}$ in (13). For resolved targets, Figure 4(d) confirms that the effect of whitening significantly improves the separability of target and background.

In both experiments, the same estimated covariance was used regardless of the percentage of background present. For this target and background, the results in Figure 4 show that, even when the background covariance is mismatched to the amount of background present, the performance still exceeds that of the SAM detector. Proper cancellation of background for hyperspectral detection is a function of the percentage of background present as well as the relationship between the target and background subspaces. Based on the LMM, this relationship will be key for

5. CONCLUSION

We have demonstrated in this paper that, under the assumption of linear mixing, detection in hyperspectral processing bears significant similarities with detection in MTI radar. The key to this parallelism is the analogous relationship between endmembers and steering vectors as well as abundances and RCS values. Our detection results indicate that statistical detectors for radar can be adapted to hyperspectral signals for both the sub-pixel and resolved target problem. even though sub-pixel targets give rise to replacement target models. Moreover, future work will continue to investigate methods for translating the optimalities of radar detection to the hyperspectral domain.

6. REFERENCES

[1] Dimitris Manolakis, Gary Shaw, and Nirmal Keshava, "Comparative analysis of hyperspectral adaptive matched filter detectors," in *Algorithms for Multispectral, Hyperspectral, and Ultraspectral Imagery VI*, Apr. 2000, vol. 4049 of *Proceedings of the SPIE*, pp. 2–17.

[2] James Ward, "Spate-time adaptive processiing for airborne radar," Tech. Rep. TR-1015, MIT Lincoln Laboratory, 1994.

[3] E. J. Kelly, "An adaptive detection algorithm," *IEEE Transactions on Aerospace and Electronic Systems*, vol. 22, no. 5, pp. 115–127, Mar. 1986.

[4] L. L. Scharf and L. T. McWhorter, "Adaptive matched subspace detectors and adaptive coherence," in *Proc. 30th Asilomar Conf. On Signals and Systems*, 1996, pp. 1114–117.

[5] C. D. Richmond, "Performance of the adaptive sidelobe blanker detection algorithm in homogeneous environments," *IEEE Transactions on Signal Processing*, vol. 48, no. 5, pp. 1235–1247, May 2000.